ZIBELINE INTERNATIONAL™ PUBLISHING

Water Conservation & Management (WCM)

DOI: http://doi.org/10.26480/wcm.01.2023.01.05

ISSN: 2523-5664 (Print)
ISSN: 2523-5672 (Online)
CODEN: WCMABD

REVIEW ARTICLE

SYNTHESIS OF ZNO DOPED MULTI WALLED CARBON NANOTUBES (MWNTS) FOR DYES DEGRADATION AND WATER PURIFICATION

Rimma N. Abdrashitova*, Galina S. Bozhenkova, Andrey A. Ponomarev, Alexandr G. Gilya-Zetinov, Alexandr A. Markov, Michail D. Zavatsky

Tyumen Industrial University, Tyumen 625000, Russia
****Correspondence address Email: abdrashitovarn@tyuiu.ru***

ARTICLE DETAILS

Article History:

Received 10 October 2022
Revised 04 November 2022
Accepted 01 December 2022
Available online 03 December 2022

ABSTRACT

Using the co-precipitation approach, multi-walled carbon nanotubes (MWNTs) doped with ZnO nanoparticles (NPs) were successfully synthesized. X-ray diffraction (XRD), scanning electron microscopy (SEM), Fourier transform infrared spectroscopy (FTIR), diffuse reflectance spectroscopy (DRS, UV-visible), and energy dispersive X-ray spectroscopy were used to examine the manufactured photocatalysts. Crystal structure, morphology, optical characteristics, optical bandgap, and elemental analysis are all determined by EDX analysis. The photocatalytic activity of the resulting photocatalysts was assessed by observing the breakdown of methyl orange methylene blue (MB) when exposed to UV and visible light. Different degradation behavior was seen for the ZnO-coated MWNTs, indicating that the MBs can fully mineralize through the post-use self-sensitized degradation process of the coated MWNTs. The created photocatalyst can be used for environmental and water cleaning.

KEYWORDS

Co-precipitation method, MB degradation, Water Purification, ZnO NPs coated MWNTs, Photocatalyst, Environmental applications

1. INTRODUCTION

Among various resources for maintenance of life, water is the most important one which man has utilized ever since. As it is not possible to exploit the water which is in the form of oceans and icecaps ~97% and our water requirements are mainly fulfilled by water from precipitation or from underground water resources. Since these resources comprise only 2-3% of total water, are limited in quantity and fastly become scarce to be used as utilizable water, although they are continually purified by natural precipitation and evaporation. Water which is indeed essential for evolution and existence of life covers almost 70% of earth. Out of that approximately 97% of water is in the oceans, remaining 2% in the form of glaciers and only 1% fresh water is available for our use (Harlang et al., 2015, Al-Kdasi et al., 2004; Srinivasan et al., 2000).

It is quite concerning that pathogenic bacteria and fungi are developing treatment resistance at an alarming rate and developing infectious illnesses. Despite growing knowledge of the etiology of microbes and the application of cutting-edge therapeutics, morbidity and mortality related to microbial illnesses remain high to this date. In 1975, out of total production (640,000 tons), over 3,60,000 tons of dyestuffs were used in the textile industry and 15% were disposed of as sewage. Many other processes, such as paper and pulp processing and foam tanning, also use large amounts of dye, increasing dye emissions. The injection of dye into this water area is also optically undesirable. Additionally, the increased antibacterial activity of composites created with metal nanoparticles and polymers may increase their usefulness. Due to its potential applications in numerous significant fields of science and technology, including gas sensors, magnetic phase transitions, catalysis, and superconductors, copper oxide (CuO) nanoparticles are of great interest. These colorful wastes are naturally toxic and carcinogenic. A significant environmental issue is the pollution of the environment by such harmful compounds. Textile dye waste can result in issues such foaming, color retention, high pH, heavy metal deposition, and swift changes in water flow. 3. Heavy metals like the dyes Cu, Co, Mg, Ni, Mn, Hg, Cd, and Cr4,5 is abundant in it. The main sources of trace metal accumulation in wastewater are floating solid particles and sediments (Khatri et al., 2012; Tyndall et al., 1993). Dissolved oxygen rapidly depletes when pollutants like chlorine and heavy metals are present, forming an "oxygen bag" in the entering water. Contaminants also reduce the water's ability to purify itself by destroying the causative microorganisms (Cofino, 1989; Ongley et al., 1992). Metallic contaminants and other contaminants also tend to persist indefinitely, circulating and it eventually accumulates throughout the food chain (Soni and Ruparelia, 2013; Sanroman et al., 2004; Solar et al., 2016).

A nearly parallel nanorod array was to be fixed to a substrate forming a collecting electrode. The surface of the nanorods effectively provides a large heterojunction area, while the metal nanorod core itself provides an optimal pathway for charge carriers to reach the underlying electrodes. So far, there are few reports on the fabrication of core-shell nanorod arrays and their use as DSSC electrodes (Zhao et al., 2004; Miao et al., 2008). AOP's photodegradation component has become a viable method for decomposing organic matter (Gomez et al., 2007; Rauf et al., 2007; Yadav et al., 2016). Due to its low cost and non-selective photocatalytic degradation, this technique is more effective than other AOPs (Arabatzis et al., 2003; Gultekin et al., 2014; Sahel et al., 2007; Mahmodi, 2014; Mahmodi et al., 2006; Krishnakanth et al., 2016). The focus of research now is to find ways to significantly oxidize these toxic substances into safe, non-toxic substances using photolytic processes that can use the sun's energy to activate them (Hoffmann et al., 1995; Okamoto et al., 2013).

Information on the mobility of ZnO is sparse, with values mainly in the range of 5–30 cm2/(V.s) (Hester, 2007). Recently, a viable alternative to TiO2 nanoparticles has been zinc oxide (ZnO) nanoparticles.

Quick Response Code	Access this article online	
	Website: www.watconman.org	**DOI:** 10.26480/wcm.01.2023.01.05

Cite The Article: Rimma N. Abdrashitova, Galina S. Bozhenkova, Andrey A. Ponomarev, Alexandr G. Gilya-Zetinov, Alexandr A. Markov, Michail D. Zavatsky (2023). Synthesis of ZNO Doped Multi Walled Carbon Nanotubes (MWNTS) For Dyes Degradation and Water Purification. *Water Conservation & Management, 7(1): 01-05.*

Carbetaamide – pesticide (Poulios, 1998), triclopyr – herbicide (Percherancier et al. 1995), treatment of wastewater from the pulp industry [29], and photolysis of various other azo dyes proved that ZnO is more efficient (Khodja et al., 2001). However, the nanoparticles thus synthesized aggregate with greater surface energy due to their larger specific surface area. Therefore, to improve dispersion, requires surface modification of ZnO nanoparticles, which have a higher value of active reaction centers than those of TiO2 (Gouvea et al., 2000).

Carbon Nanotubes (CNTs) are hollow nano-cylinders made of graphitic micro-crystals that have unique features and can carry electricity at ambient temperature with almost little resistance (O'regan and Gratzel, 1991; Ma et al., 2014). Single-walled carbon nanotubes (SWNTs) and multi-walled carbon nanotubes are the two main types of carbon nanotubes that have acquired a higher level of structural perfection (MWNTs) (Gerard et al., 2002). Laser ablation, arc discharge, and chemical vapor deposition are examples of CNT synthesis techniques (CVD). Recently, 20 cm long CNTs were arranged by using catalytic pyrolytic cleavage of n-hexane by the suspension method (Xu et al., 2002; Wang et al., 2017).

Linqin Jiang et al. presented a ZnO/MWNTs nanocomposite was made using a non-covalent technique, and the methylene blue (MB) solution revealed that its absorption spectra was blue-shifted, most likely due to quantum confinement. He disintegrated in 2.5 hours. 38–40 at UV illumination His TiO2 (anatase)-coated MWNTs as nano photocatalysts were made by Guimin et al. and colleagues by hydrolyzing titanium iso propoxide in supercritical ethanol. When exposed to visible light, phenol broke down, and the nanocomposites had greater activity (92.4% at 8 hours) than mechanical mixtures of MWNTs and TiO2 and pure TiO2. Li et al. created the polyol technique. Create MWCNTs with a CdS coating. Brilliant Red X-3B, an azo dye, was exposed to visible light to cause photolysis. According to first-order kinetics analysis, ag deposition improved the activity of MWNT/TiO2 photocatalysts and the pace of the photocatalytic process (1.2-fold). Here, we described a straightforward technique for producing multi-walled carbon nanotubes (MWCNTs) and measuring their individual catalytic efficiencies to increase their photocatalytic efficiency.

Nanoparticles were effectively implanted onto the surface of (MWCNTs) to enhance catalytic proficiency. In addition, metal oxide nanoparticles are loaded into a pre-obtained nanocomposite material (MWCNT) and obtained (MWCNT). This further improves the catalytic efficiency of the designed photocatalyst. The synthesized photocatalyst might have applications in water purification and in environment cleaning applications.

2. Characterization Techniques Details

Utilizing X-ray diffraction (XRD) analysis, which is based on the dual characteristic I one can learn more about the structural characteristics of the compounds' crystallinity and both a particle and a wave nature. Incident radiation is both partially absorbed and dispersed. This theory states that incident and scattered light fluxes act perpendicularly, albeit in opposing directions, on the surface of powdered materials. The scattered light from the test substance is collected with an integrating sphere, and the collected light is detected. The diffuse reflectance that results for infinitely thick materials can be understood as the relationship between the absorption coefficient (K) and the scattering coefficient (S) according to the Kubelka-Munk function. Using a Nicole FTIR Nexus 470 spectrometer in dry conditions, the FTIR spectra were captured. The rotation and vibration of chemical bonds in infrared-absorbing bipolar compounds serve as the basis for FTIR investigation. The strength and configuration of chemical connections between atoms in molecules directly affects the intrinsic frequency modes (rotations and vibrations) of those atoms. The result is a distinctive band pattern, known as H. 4000-400/cm, in the middle of the IR spectrum, which is additionally employed for material quantification and qualifying. The foundation of DRS is the light scattering of substances in the UV (10-400 nm), visible (400–780 nm), and NIR (780–2400 nm) ranges. DRS basically counts the amount of light scattered from an infinite layer and compares it to the amount of light scattered from a reference material that is undamaged, non-absorbing, and has a thickness of at least 2-3 nm. This percentage is calculated based on wavelength. The scattered light from the object under study is gathered by an integration sphere, and the collected light is then detected. To learn more about the material being studied, the EDX device is connected to the scanning electron microscope.

3. Experimental Scheme and Methodologies

3.1 Materials and Reagents

Co-precipitation was used to create nanocomposites of multi-walled carbon nanotubes (MWNTs). Locally purchased MWNTs were used to create nanocomposites. An agent for precipitation was NaOH. Using HCl, H2SO4, and HNO3, MWNTs were purified and functionalized. The model textile dye used was methylene blue (MB). All chemicals and reagents were used without further purification, except for MWNTs. The whole experimental process is schematically represented in Scheme 1.

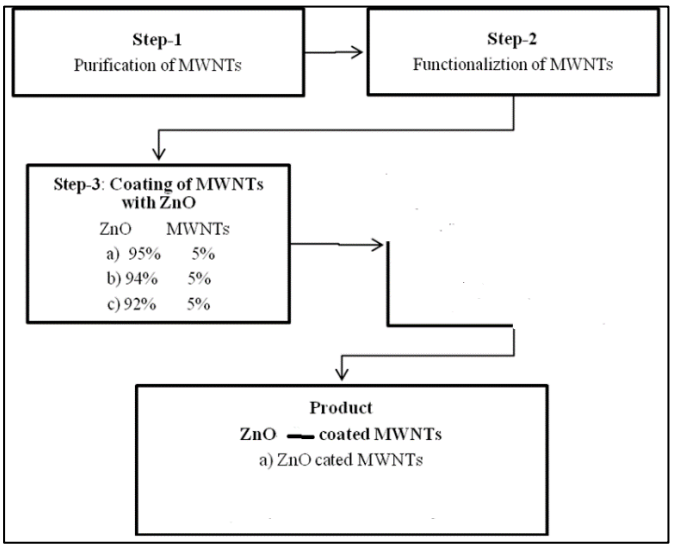

Scheme 1: The schematic representation of the experimental work

3.2 Synthesis of ZnO Coated MWNTs

The ZnO-coated MWNTs were created using a co-precipitation technique. For 30 minutes, sonication was used to disperse functionalized MWNTs in deionized water. According to the schematic in Scheme 2, the necessary quantity of Zn(NO3)2 6H2O for ZnO-coated MWNTs with various compositions was dissolved in 20 mL of deionized water. Dropwise additions of the Zn(NO 3) 2.6H 2 O solution were made while continuously swirling the MWNT dispersion on the heated plate.

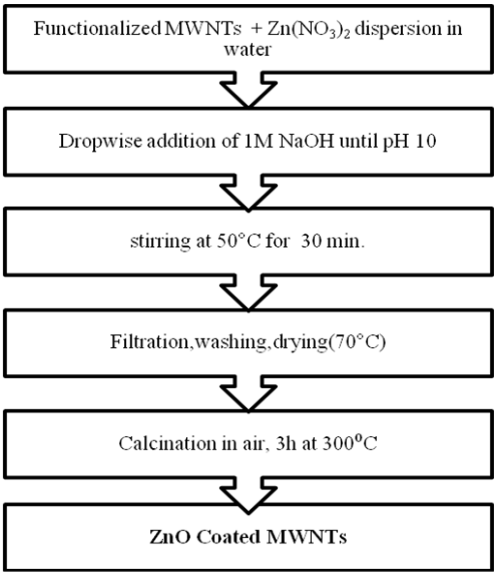

Scheme 2: Schematic framework of ZnO coating of MWNT

To bring the pH of the dispersion to 10, a NaOH solution was added dropwise while stirring, precipitating Zn(OH) 2. For homogeneity, stirring was kept up for a further hour. To give the precipitate time to settle, the mixture was aged for one night. The precipitate was then rinsed with extra distilled water and filtered using #40 Wattman filter paper to get rid of the dissolved nitrates. To verify that nitrate had been removed, a ring test was conducted. The precipitate was calcined at 350°C, the ideal calcination temperature, and dried at 70°C. A schematic is shown in Scheme 2.

3.3 Photocatalytic Activity Determination

Methyl orange was independently degraded under UV (280 nm) and visible light (480 nm) irradiation to measure the photodegradation efficiency of the catalyst so produced. Figure 3 depicts the experimental

configuration. 6. In quartz jars with 50 mL of dye suspension and 50 mg of catalyst in aqueous solution at room temperature and vigorous stirring, photocatalytic tests were carried out. The absorbance at max (462 nm) of a 50-ppm suspension of methyl orange in distilled water was measured using a UV-Vis spectrophotometer (Perkin-Elmer UV/Vis Spectrometer λ 25), and this absorbance was normalized. To allow the adsorption-desorption equilibrium to be formed on the catalyst surface, 50 mg of the photocatalyst thusly created was added to the methyl orange mixture and agitated for an hour in the dark prior to exposure. A UV-visible spectrophotometer was used to measure the absorbance at maximum to determine the methyl orange content. The suspension was then exposed to both visible and ultraviolet (280 nm) light independently (480 nm).

4. Results and Discussion

Figure 1 displays the X-ray diffraction spectra of unfunctionalized multiwalled carbon nanotubes and pristine multiwalled carbon nanotubes (A). Purification and functionalization of the original MWNTs resulted in the disappearance of the intensity and those of 2 = 51.30 and 76.20, and the appearance of the MWNTs' distinctive diffraction peaks at 2 = 25.580 (002) and 43.350 (100). Impurity peaks are not visible, as seen in Figure 1(b).

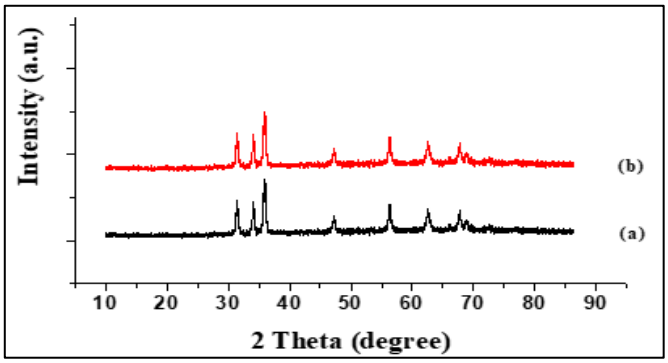

Figure 1: X-ray diffraction spectra of (a) ZnO (b) 95%ZnO: 5%CNTs.

Figure 1 (a) displays the XRD pattern of pure ZnO that was calcined at 300°C for three hours. The crystalline wurtzite structure corresponds to the distinctive hexagonal. Figure 1(b) displays the nanocomposite that was calcined at 300 °C for three hours (b). Since the XRD method is sensitive to concentrations above 3%, the low NiO concentration prevents the typical NiO peaks from being visible in the XRD spectra of the nanocomposites. Additionally, the MWNTs' diffraction peaks are spectra from da Less crystalline than ZnO, MWNTs overlap with the strong ZnO peaks during complex formation of ZnO because of this. By using the Scherer formula to enlarge the diffraction peaks, it is possible to determine the ZnO crystallite size,

$$D = \frac{0.9\lambda}{\beta COS\theta} \quad (1)$$

Where,

D= The particle size in nm

λ= Wave length of the X-ray source (Cu Kα = 1.542 Aº)

β= Full Width at Half Maximum (FWHM)

Θ=Tithe diffraction angle

The FWHM of ZnO was used to determine the particle sizes of ZnO and ZnO contained in the nanocomposites, which are displayed in Table 1. MWNT regulates the size of ZnO nanoparticles attached to surfaces.

Table 1: Particle Size of Zno and Arranged Nanocomposites Calculated Using Scherer Formula

Sr. No.	Composition	Crystallite size (nm)
1	ZnO	48.9
2	95%ZnO:5%CNTs	27.9

4.1 Scanning Electron Microscopy (SEM) Analysis

For morphological analyses, scanning electron microscopy (SEM) analysis was carried out. Photomicrographs of functionalized MWNTs, ZnO and ZnO-coated MWNTs are presented in Fig. 2(a and b), and NiO-ZnO-coated MWNTs (1%, 3rd) exhibits micrographs (a-b). SEM micrographs of the functionalized MWNTs show that the MWNTs range in diameter from 35 to 50 nm and that they are deagglomerated and have clean surfaces, suggesting effective cleaning and oxidation treatments.

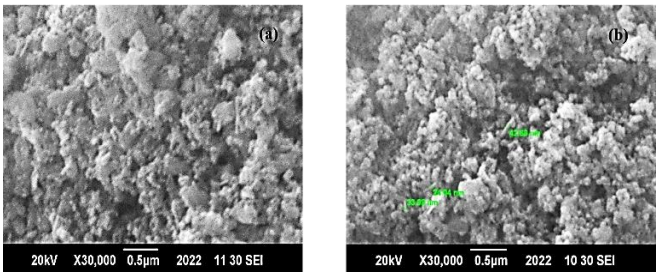

Figure 2. Scanning electron microscopy images (a) ZnO NPs pristine (b) 95% ZnO: 5%MWNTs.

However, incorporation in the form of nanocomposites demonstrates that ZnO grown on the defect's sites created by oxidation treatment on the surface of MWNTs, have uniformly and homogeneously distributed ZnO nanoparticles. SEM micrographs of ZnO show an inhomogeneous shape and size of nanoparticles.

4.2 Fourier Transform Infra-Red Spectroscopy (FTIR)

To control surface functional groups, Fourier transform infrared (FTIR) spectroscopy was developed. Figure 3 displays the FTIR spectra of the produced nanocomposites coated with ZnO NPs and the functionalized MWNTs.

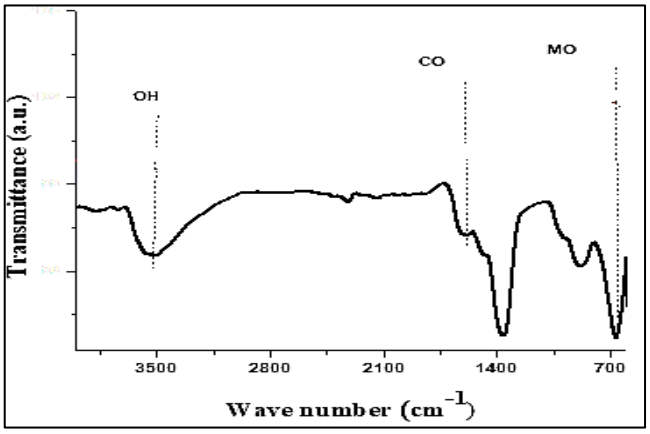

Figure 3. FTIR spectra of 95%ZnO: 5%MWNTs.

The FTIR spectrum of the functionalized MWNT shows that the carbonyl stretches (-C=O) at 1720 cm-1 has a low intensity peak and the hydroxyl functional group (-OH) has a high intensity peak at 3428 cm-1. A second absorption peak at 1655 cm-1 is linked to the carbonyl stretching that can be identified as the C-O stretching from the quinine ring structure of the oxidized MWNTs, and the (-) of the carboxyl group is characteristic COOH) of these materials. The lactone or phenol group's C-O or C-C expanse is attributed a large peak at 1217 cm -1. The high-intensity peaks of MWNTs loaded with ZnO in the composites suggest that MWNTs and ZnO have formed polar connections through oxygen-containing groups. As a result, the absorption strength rises, and the frequency of the absorption moves to higher wavenumbers. Due of the stronger C-O-Zn bond, the C=O stretching frequency changes from 1665 cm-1 to 1690 cm-1. The ZnO NPs have a distinctive metal oxide peak at 659 cm-1.

4.3 Diffuse Reflectance (DRS UV-visible) Spectroscopy Analysis

We determined the optical bandgap energy of ZnO and nanocomposites having various concentrations of ZnO, NiO, and MWNTs using diffuse reflectance spectra. Figure 4 displays the corresponding graphs and their make-up (a and b, respectively). The bandgap energies were determined using the Kubelka-Munk function-related equations listed below:

$$F(R) = \frac{(1-R)^2}{2R} \quad (4.2)$$

Where 'R' is the absolute reflectance of the samples and F(R) is the Kubelka-Munk function for the direct band gap semiconductor as ZnO is a direct band gap material.

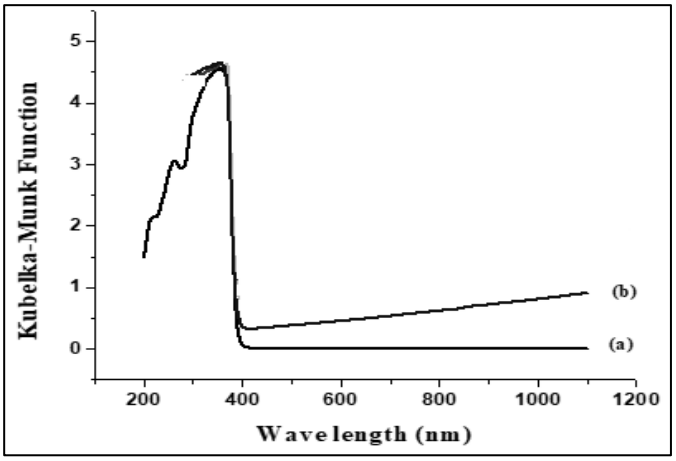

Figure 4. DRS UV-visible spectra of (a) ZnO NPs (b) 95%ZnO: 5%CNTs.

The band gap energies thus calculated for ZnO and the nanocomposites by using the relation Ebg= 1240/λ (nm) are given in Table 2.

Table 2: The Band Gap Energies of Zno and Prepared Nanocomposites Using Kubelka-Munk Function

S. No.	Composition	Band gap energy (eV)from DRS
1.	ZnO	3.30
2.	95% ZnO: 5% CNTs	3.23

4.4 Energy Dispersive X-ray Spectroscopy (EDX) Analysis

By using EDX, the thusly created nanocomposites underwent elemental analysis. The EDX spectrogram of functionalized MWNTs covered with ZnO NPs is shown in Figure 5. The EDX results show that the only elements present in the functionalized MWNTs are 'C' and 'O'. For complexes, C, O, and Zn peaks are present, confirming complex formation. As the NiO concentration increases, so does the intensity of the Ni peak. The results demonstrate remarkably consistent behavior between the finished product's actual composition and the composition that was employed in the experiment. Because NiO (0.24%), an impurity, is found in the EDX spectra of ZnO-coated MWNTs due to an experimental error, there is a discrepancy.

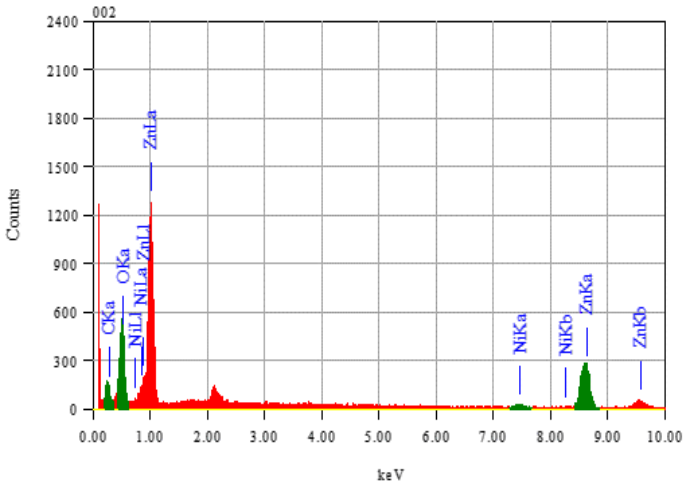

Figure 5: Energy dispersive X-ray (EDX) spectrographs of 95%ZnO: 5%MWNTs.

4.5 Photocatalytic Activity Determination

Under UV (282 nm) and visible light (490 nm) irradiation, the photocatalytic activities of functionalized MWNTs, ZnO, ZnO-coated MWNTs, and ZnO/NiO-coated MWNTs demonstrated their potential as model fiber dyes. as indicated by methyl orange photolysis (MO). Monitoring the absorbance of solution sample samples at the wavelength of maximum absorbance (max) at 462 nm allowed researchers to measure the amount of residual methyl orange in solution after irradiation for 30 min for 6 h at pH=7. A quartz spectroscopic cuvette with a 1 cm pathlength was used to measure the maximum absorption wavelengths at room temperature and pressure.

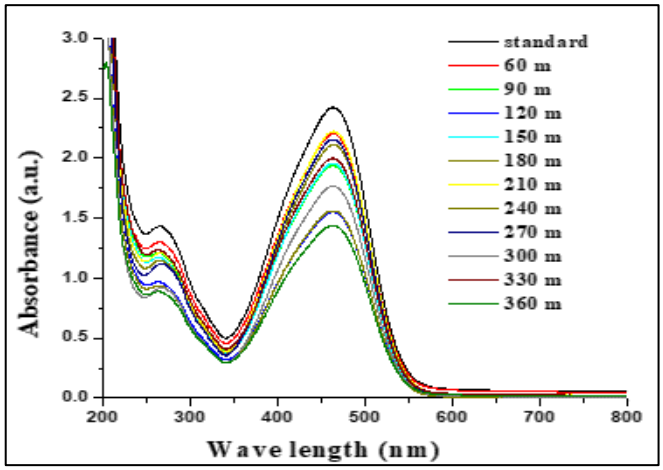

Figure 6: The photodegradation progress of methyl Blue using 95%ZnO coated MWNTs under UV (284 nm) and visible light (479 nm) irradiation.

The functionalized MWNTs' (FCNTs') absorption spectra revealed a slight reduction in max in both the UV and visible ranges, but the reduction was more pronounced for reactions that took place during the first hour (without irradiation), and there was no discernible reduction in after that. max is reached, showing that functionalized MWNTs (FCNTs) are more efficiently absorbed yet ineffective as a photocatalyst for the breakdown of methyl orange. Figure 6 illustrates that for ZnO, methyl orange degradation was more pronounced under UV light than under visible light. Because high-energy UV photons are more effective at destroying the dye than visible light, for methyl ZnO, the orange color loss was greater under UV than under visible light. The photolysis was higher when ZnO was loaded onto the surface of functionalized MWNTs than when ZnO and MWNTs were utilized separately, suggesting that MWNTs increase ZnO's capacity for photolysis. Electrons are excited by UV light and go to her ZnO conduction band, where they eventually end up in MWNTs. Due to the reduced recombination of electrons and holes caused by MWNTs' electrical conductivity, the photocurrent in the composites and activity are boosted.

4.6 Kinetics of Methyl Orange Degradation

According to the Langmuir-Hinshel-Wood model, heterogeneous photocatalysis occurs at a constant rate. This suggests that the pseudo-first-order kinetics of the breakdown of methyl blue: $\ln(C_0 / C) = k_{app} t$ (3)

Where 'kapp' is the apparent rate constant for pseudo first order reaction, 'Co' is the initial concentration of the aqueous solution of methyl orange and 'C' is its concentration after time 't'.

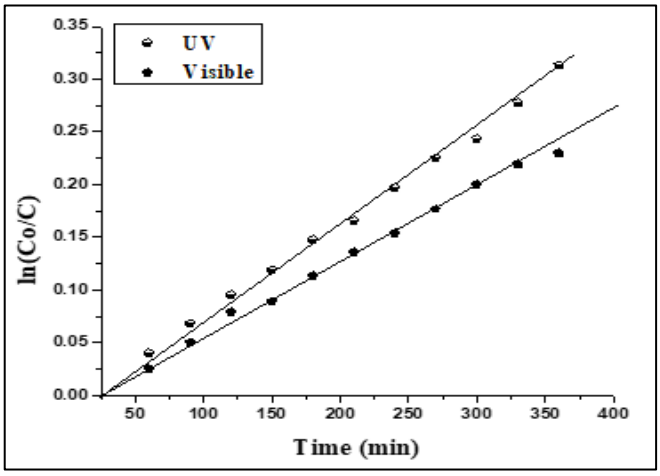

Figure 7: Kinetics of photodegradation of methyl orange using ZnO coated MWNTs under UV (284 nm) and visible light (479 nm) irradiation.

The slope of the line, obtained by plotting ln(C0/C) versus t, indicates the rate constant's value. Figure 7 displays plots of ln (Co/C) against "t" for ZnO, ZnO-coated MWNTs, 1% NiO-coated MWNTs, and 3% NiO-coated MWNTs. It turns out that modifying photocatalysts with MWNTs and a tiny amount of ZnO NPs is an easy way to effectively destroy MB pigments and

organic contaminants when exposed to visible light. This technique might work best for getting dye out of materials. The synthesized photocatalyst may be applied to water purification and environmental purification.

5. Conclusion

By using the co-precipitation approach, composites of ZnO-coated MWNTs that function as photocatalysts have been effectively created and thoroughly described. Studying the photodegradation of methyl orange under UV and visible light irradiation for the breakdown of MB dye as a model example allowed researchers to assess the photocatalytic activity of the photocatalyst. For comparative research, ZnO NPs were also produced using the same technique. According to the findings, the photocatalyst is functional in both the ultraviolet and visible light spectrums, but its photocatalytic activity is higher in the presence of ultraviolet light.

After coating acid oxidized, He MWNTs with ZnO NPs, the degradation rate increased compared with that of bare ZnO NPs. Moreover, when ZnO NPs were put onto the surface of MWNTs, the rate of photocatalytic degradation was increased. It turns out that modifying photocatalysts with MWNTs and a tiny amount of ZnO NPs is an easy way to effectively destroy MB pigments and organic contaminants when exposed to visible light. The removal of fabric color may benefit the most from this technique. The synthesized photocatalyst could also have applications in water purification as well as in environmental cleaning.

Acknowledgements

The article was prepared within the state assignment in science for scientific projects carried out by teams of youth laboratories of educational institutions of higher education subordinated to the Ministry of Education and Science of Russia under the project: "Development of domestic active bases and ready-made compositions of chemical reagents for special geological and field conditions of oil and gas production enterprises" (№ FEWN-2022-0002, 2022-2024).

References

Al-Kdasi, A.; Idris, A.; Saed, K.; Guan, C. T. 2004. Global Nest: the Int. J, 6 (3), 222–230.

Anjaneyulu, Y.; Sreedhara Chary, N.; Samuel Suman Raj, D. 2005. Reviews in Environmental Science and Biotechnology, 4 (4), 245–273.

Arabatzis, I. M.; Stergiopoulos, T.; Andreeva, D.; Kitova, S.; Neophytides, S. G.; Falaras, P. 2003. Journal of Catalysis, 220 (1), 127–135.

Cofino, W. P. 1989, 308 (November 1988), 295–308.

Gerard Lavin, J.; Subramoney, S.; Ruoff, R. S.; Berber, S.; Tománek, D. 2002. Carbon, 40 (7), 1123–1130.

Gómez-Carrasco, S.; Aguado, A.; Paniagua, M.; Roncero, O. 2007. Journal of Photochemistry and Photobiology A: Chemistry, 190 (2–3), 145–160.

Gouvêa, C. a; Wypych, F.; Moraes, S. G.; Durán, N.; Nagata, N.; Peralta-Zamora, P. 2000. Chemosphere, 40 (4), 433–440.

Gültekin, A.; Karanfil, G.; Özel, F.; Kuş, M.; Say, R.; Sönmezoğlu, S. 2014. Journal of Physics and Chemistry of Solids, 75 (6), 775–781.

Harlang, T. C. B.; Liu, Y.; Gordivska, O.; Fredin, L. A.; Ponseca, C. S.; Huang, P.; Chábera, P.; Kjaer, K. S.; Mateos, H.; Uhlig, J.; Lomoth, R.; Wallenberg, R.; Styring, S.; Persson, P.; Sundström, V.; Wärnmark, K. 2015. Nature Chemistry, 7 (11), 883–889.

Hester, D. M. 2007. Theoretical Medicine and Bioethics, 28 (5), 357–372.

Hoffmann, M. R.; Martin, S. T.; Choi, W.; Bahnemann, D. W. 1995. Chemical Reviews, 95 (1), 69–96.

Jones, F. E.; Harris, G. L. 1992. Journal of Research of the National Institute of Standards and Technology, 97 (3), 335.

Khatri, Z.; Memon, M. H.; Brohi, K. M. 2012.

Khodja, A. A.; Sehili, T.; Pilichowski, J.-F.; Boule, P. 2001. Journal of Photochemistry and Photobiology A: Chemistry, 141 (2–3), 231–239.

Krishnakanth, R.; Jayakumar, G.; Irudayaraj, A. A.; Raj, A. D. 2016. Materials Today: Proceedings, 3 (6), 1370–1377.

Liao, D. L.; Badour, C. A.; Liao, B. Q. 2008. Journal of Photochemistry and Photobiology A: Chemistry, 194 (1), 11–19.

Ma, L.; Jia, I.; Guo, X.; Xiang, L. 2014. Chinese Journal of Catalysis, 35 (2), 108–119.

Mahmoodi, N. M. 2014. Fibers and Polymers, 15 (2), 273–280.

Mahmoodi, N. M.; Arami, M.; Limaee, N. Y.; Tabrizi, N. S. 2006. Journal of Colloid and Interface Science, 295 (1), 159–164.

Miao, X.-M.; Yuan, R.; Chai, Y.-Q.; Shi, Y.-T.; Yuan, Y.-Y. 2008. Journal of Electroanalytical Chemistry, 612 (2), 157–163.

O'Regan, B.; Gratzel, M. 1991. Letters to Nature, 353, 737–740.

Okamoto, H.; Futai, M.; Medical, I.; Motor, R.; 2013. V-atpase, T. Encyclopedia of Biophysics.

Ongley, E. D.; Krishnappan, B. G.; Droppo, G.; Rao, S. S.; Maguire, R. J. 1992. Hydrobiologia, 235–236 (1), 177–187.

Percherancier, J. P.; Chapelon, R.; Pouyet, B. 1995. Journal of Photochemistry and Photobiology, A: Chemistry, 87 (3), 261–266.

Poulios, I.; Kositzi, M.; Kouras, A. 1998. Journal of Photochemistry and Photobiology A: Chemistry, 115 (2), 175–183.

Rauf, M. A.; Bukallah, S. B.; Hamadi, A.; Sulaiman, A.; Hammadi, F. 2007. Chemical Engineering Journal, 129 (1–3), 167–172.

Sahel, K.; Perol, N.; Chermette, H.; Bordes, C.; Derriche, Z.; Guillard, C. 2007. Applied Catalysis B: Environmental, 77 (1–2), 100–109.

Sanromán, M. A.; Pazos, M.; Ricart, M. T.; Cameselle, C. 2004. Chemosphere, 57 (3), 233–239.

Solár, J.; Janiga, M.; Markuljaková, K. 2016. Polish Journal of Environmental Studies, 25 (1), 291–300.

Soni, B. D.; Ruparelia, J. P. 2013. Procedia Engineering, 51, 335–341.

Srinivasan, M.; Natarajan, K.; Nagarajan, G. 2000. Bioprocess Engineering, 22 (3), 0267–0273.

Tyndall, R. M.; Marriott, R.; Valley, C.; November, I. 1993.

Wang, Y.; Zavalij, P.; Eichhorn, B. 2017. Chem. Commun., 9–11.

Xu, X.; Maclean, E. J.; Teat, S. J.; Nieuwenhuyzen, M.; James, S. L. 2002, 78–79.

Yadav, H. M.; Kolekar, T. V.; Barge, A. S.; Thorat, N. D.; Delekar, S. D.; Kim, B. M.; Kim, B. J.; Kim, J. S. 2016. Journal of Materials Science: Materials in Electronics, 27 (1), 526–534.

Yeber, M. C.; Rodríguez, J.; Freer, J.; Baeza, J.; Durán, N.; Mansilla, H. D. 1999. Chemosphere, 39 (10), 1679–1688.

Zhao, W.; Ma, W.; Chen, C.; Zhao, J.; Shuai, Z. 2004. Journal of the American Chemical Society, 126, 4782–4783.